

Article

Intrinsically Multi-Color Device Based on Dynamic Cooperation of Molecular Switches and Metal Ions

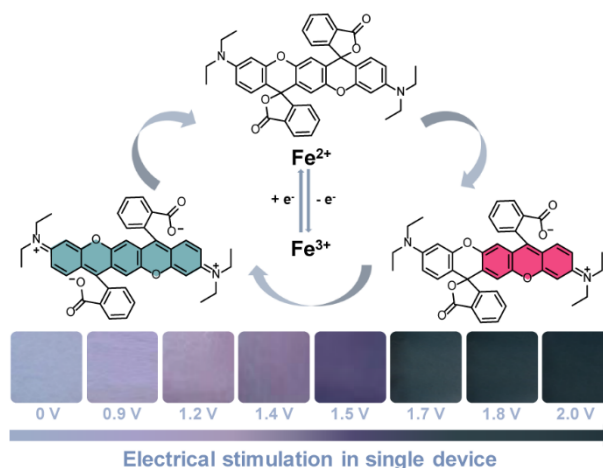
Min Li, Shuo Wang *, Ruipeng Shen, Yigui Xie, Yu-Mo Zhang, and Sean Xiao-An Zhang *

State Key Laboratory of Supramolecular Structure and Materials, College of Chemistry, Jilin University, Changchun 130012, China

* Correspondence: wangshuo@jlu.edu.cn (S.W.); seanzhang@jlu.edu.cn (S.X.-A.Z.)

Received: 6 January 2025; Revised: 5 February 2025; Accepted: 11 February 2025; Published: 19 February 2025

Abstract: Multi-color electrochromic material is a long-expected and extremely challenging material, which is important for electrochromic technology to be applied in adaptive camouflage, augmented reality, transparent display, etc. Here, an intrinsically multi-color indirect-electrochromic material based on supramolecular interactions of unusual multi-state molecular switch and metal ion was developed, combining the advantages of multi-state of molecular switch and chemical stability of metal ion. Related prototype device, with transparent intrinsic colorless, magenta, cyan and various mixed colors, have been explored and demonstrated. The mechanism was based on the dynamic coordination of multiple metal ions and single-molecular-dual-switches within fragile supramolecular clusters. Wherein, the color and lightness could be controlled simply by the bias applied, with abilities such as transmittance change (41%), coloring time (7.8 s), coloration efficiency (>100 cm²/C), and reversibility (>600 test cycles, no abnormal changes). The prototype device was fabricated to show the potential to be used in low energy consumption display.



Keywords: electrochromism; intrinsic multi-color device; leuco dye; metal ion; dynamic coordination

1. Introduction

Electrochromic (EC) materials have the unique property of optical change after redox reaction [1]. They have been partially applied in scenarios like rearview mirror and smart window in cars and airplanes [2,3]. Compared to the common single-color change, EC materials with multi-color change are very beneficial and required. The emerging multi-color ability is becoming more and more important for EC materials to be applied in broader fields, such as adaptive camouflage [4–9], augmented reality [10,11], transparent display [12–15], optical information encryption [16] and so on. Related multi-color electrochromic device (ECD) has been extensively studied and developed so far. Many of them were developed through the combination of multiple kinds of single-color EC materials or by lateral/vertical arrangement of them. Hereinto, multi-color EC materials have broad development prospects in related ECD. These materials show multi-color under different bias, obviously no complex combination or arrangement of single-color EC materials are needed to develop more ideal multi-color ECD.

Known multi-color EC materials need multi-redox states to cause structural change to result in multi-color, researchers developed them so far through the following ways. For single compound, many pleasant colors were developed by finely designed molecules with multi-redox-state. Impressive various multi-color EC materials were developed through this way, like viologen (derivative) [17–20], vanadium oxide [12,21] and methyl ketone (derivative) [22]. Through the tailoring of different EC blocks, the ECDs also show multi-color electrochromism of the blocks, like the copolymerization of triphenylamine and viologen [23], the co-assembling of tungsten oxide and vanadium oxide [24]. This method cleverly combines the advantages of different EC blocks. Besides, by



constructing the trilayer film structure driven by discharging/self-charging mechanism, intrinsic multi-color electrochromism can also be realized [25]. And the hybrid materials of metal ion and ligand have also realized intrinsic multi-color electrochromism. It's realized through the mixture of different metal ion centers like Os^{2+} , Co^{2+} , Fe^{2+} , Ru^{2+} and pyridine derivatives [26,27], or by forming supramolecular polymer of them [7]. Wherein multi metal ion centers offer multi states of metal-to-ligand charge transfer (MLCT) to realize multi-color electrochromism. In addition, interesting structural color has also been induced into ECD to realize multi-color, like the localized surface plasmon resonance (LSPR) of silver nanoparticles [28,29] and Fabry-Perot (F-P) nanocavity of metal tungsten [30]. Structural color provided novel perspective of EC mechanism and materials with rich colors.

It should acknowledge that these preliminary works have demonstrated various useful methods and unique multi-color transformation functional attributes. They have greatly expanded the available methods and development prospects in this field. However, ideal multi-color EC materials are still challenging due to the traditional ways' technical barriers such as EC mechanisms, complex synthesis and fabrication processes. Development of a simple and effective method to achieve high molar absorptivity and multiple colors of organic small molecules for the preparation of more ideal EC materials has been long-awaited.

Based on this challenge, we developed herein a new EC material with intrinsic multi-color, based on dynamic coordination of multiple ions and multi-state-molecular-switches. Unlike common direct EC materials, their chromophores undergo direct color change due to redox reactions, the electrochromism in this work is indirect way of color change. Herein, multi-valence metal ion was used as redox center to provide multi-valence state. Meanwhile, the relevant color switching unit is the cis-ABPX with multi-color states, which has recently been discovered and demonstrated by admirable research groups [31,32] and possesses unique other properties. The color change of this EC system is introduced indirectly by redox of metal ions first and then dynamic coordination of multiple related metal ions with the cis-ABPXs. This special design brought many advantages, the redox center was inexpensive and chemically very stable, and the color-switching unit was easily synthesized and modified. In addition, the EC system is endowed with high molar absorbance coefficient cis-ABPX, thereby achieving high coloration efficiency (CE). Here, adjustable Fe^{2+} was used as an example, to act as the expected redox center to dynamically coordinate with the dual-switchable rhodamine derivative cis-ABPX. The colors of the EC system could be finely regulated under different bias. Compared with previous work, this work realized multi-color electrochromism within single molecular switch, and the multiple colors and their absorption intensity could be precisely controlled at the same time by voltage in this work.

The color regulation of cis-ABPX was systematically explored, and how to distinguish different color states from chemical stimulus to electrical stimulus was demonstrated. Then its EC mechanism based on dynamic cooperation was given. Thereafter, by optimizing the fabrication process of ECDs, prototype ECDs were fabricated to demonstrate their multi-color ability. The ECD was possible to switch between colorless, magenta, cyan and various mixed colors with different metal ions and cis-ABPXs condensed states. Those intrinsic color changes were purely realized in single pixel of above complex, without traditional pixel arrangement in vertical or lateral way. The success and gains from this exploration based on dynamically coordinated single-molecule multicolor changes may inspire and motivate more researchers to adopt similar strategies to accelerate the development of intrinsic EC materials, and future application in transparent displays and many other low-energy application scenarios.

2. Experimental Part

2.1. Materials and Instruments

4-diethylamino-ketoacid (99%), methyl sulfonic acid (MSA, 99%), anhydrous sodium carbonate (A.R.), anhydrous sodium sulfate (A.R.), FeCl_3 (95%), FeCl_2 (99%), trifluoroacetic acid (TFA, 99%), p-benzoquinone (BQ, 98%), hydroquinone (HBQ, 99%), propylene carbonate (PC, 99.5%) were purchased from Energy Chemical Company (Shanghai, China). Polymethyl methacrylate (PMMA, M_w : ~100,000), chromatographic pure acetonitrile, dichloromethane, methanol, tetrahydrofuran (THF) and tetrabutylammonium hexafluorophosphate (TBAPF₆, 98%) were purchased from Aladdin Reagent. Trichloromethane was purchased from China National Pharmaceutical Group Corporation. TBAPF₆ was recrystallized three times in ethanol and dried under vacuum overnight at 80 °C.

¹H NMR spectra were obtained on a AS 400 400M (Q.NE Instruments Ltd., Wuhan, China) and referenced to tetramethyl silane (TMS) as an internal standard. Ultraviolet-visible absorption spectra were obtained on the double-beam UV-2600i spectrophotometer (Shimadzu, Suzhou, China) or SPECORD 210 PLUS (Analytikjena, Jena, Germany). High-resolution mass spectra (HRMS) were measured on Agilent 1290-microTOF-Q II. MALDI-

TOF mass spectrometry were measured on a Bruker Autoflex speed TOF. Fourier Transform infrared spectroscopy (FT-IR) was measured on a Vertex 80/80 V FT-IR spectrometer, which used LN-MCT Mid DC detector in the range of 4000–400 cm^{-1} wave numbers. Unless otherwise mentioned, the electrochemical experiments were measured using the SP-150 Electrochemical Workstation (Bio-Logic) at room temperature.

2.2. Synthesis of *cis*-ABPX

cis-ABPX was synthesized according to Uchiyama et al.'s work [30]. The synthesis route of *cis*-ABPX is shown as Figure S1. Both 4-diethylamino-ketoacid (620 mg, 2.0 mmol) and HBQ (110 mg, 1.0 mmol) were placed in a 15 mL pressure tube. MSA (5 mL) was added and heated at 110 °C for 4 h. After cooling to room temperature, the reaction mixture was added to saturated sodium carbonate aqueous solution, then the solution was extracted with CH_2Cl_2 for 3 times, and then dried with anhydrous sodium sulfate. The solvent was evaporated to form dark purple solid. The crude product was purified by silica gel chromatography and eluted with $\text{CH}_2\text{Cl}_2/\text{MeOH}$ (100:1) to obtain product, which was pink powder, with yield of 24.0%. The product was characterized by nuclear magnetic resonance (NMR) spectroscopy (Figure S2), high-resolution mass spectrometry (HRMS, Figure S3) and MALDI-TOF mass spectrometry (Figure S4). More details about NMR and mass spectrometry are provided in supporting information.

2.3. Preparation of the Solution

The electrochromic solution was a mixture of *cis*-ABPX (13.28 mg), FeCl_2 (6.3 mg), TBAPF_6 (75 mg), PMMA (150 mg) and PC (75 mg) in 1.0 mL THF and was stirred for 2 h. The conducting solution was a mixture of PMMA (1.94 g), TBAPF_6 (0.97 g) and PC (0.97 g) in 15 mL acetonitrile and was stirred for 2 h. The ion storage solution was a mixture of PMMA (1.94 g), TBAPF_6 (0.97 g), PC (0.97 g), BQ (0.16 g) and HBQ (0.33 g) in 30 mL acetonitrile and was stirred for 2 h.

2.4. Device Fabrication

The transparent electrochromic film was spin-coated (2000 r.p.m., 15 s) on the first ITO electrode. The ion storage film was coated on the second ITO electrode and the height of the scraper was set to 1300 μm and 1400 μm , respectively. The conducting film was then coated on the top of the ion storage film and the height of the scraper was set to 1500 μm , 1600 μm , 1700 μm , 1700 μm , 1800 μm , 1800 μm , respectively. Both ITO electrodes were assembled together.

2.5. Visible Absorption Spectrum Test

All in-situ absorption spectra during the voltage stimulation were tested in a cell of in situ three-electrode system under room temperature (25 °C), with TBAPF_6 as the electrolyte. Air was used as reference for the measurements, and the optical path of the sample cell was 1 mm.

2.6. Calculation of the CE and the Response Time

CE is defined as the change in absorbance (ΔA) obtained by injecting a certain amount of charge per unit area. The CE herein was tested in ECD and calculated according to the formula: $\text{CE} = \Delta A/Q$. Air is used as a reference for absorption measurements. In Figure 4c, the conversion of A and T was achieved according to the formula: $A = Lg(1/T)$.

The response time denotes as the time required for an electrochromic material or device to complete 90% of its optical modulation. For Figure 4c, with “bleached state to colored state” switching, the response time can be divided into coloring time (t_1) and fading time (t_2).

3. Results and Discussion

To realize intrinsic multi-color electrochromism in single pixel, the rhodamine derivative *cis*-ABPX was chosen as the coloring unit in our EC system. *cis*-ABPX is a sensitive molecular switch, and due to its molecular tautomerization, it has color changing in response to external stimuli, including protonation effect, photochromism and piezochromism [33]. Two lactone rings of *cis*-ABPX brought it multi-state ability, under the treatment of proton (TFA) in the solution, several absorption peaks appeared due to the opening of two spirolactone rings (Figure 1a), the spectral change here was in agreement with the pioneers [30], and its structure change was proved by $^1\text{H-NMR}$ (Figure S5). *cis*-ABPX formed monocation to show magenta under the stimulation of proton, and then formed dication to show cyan under more amount of proton (Figure 1a). It's always more difficult to form

dication than monocation of it, which meant its state/color could be distinguished by the amount of proton. But cis-ABPX needed extreme amount of proton to form dication to show cyan, even 600,000 eq. was needed to reach maximum coloration.

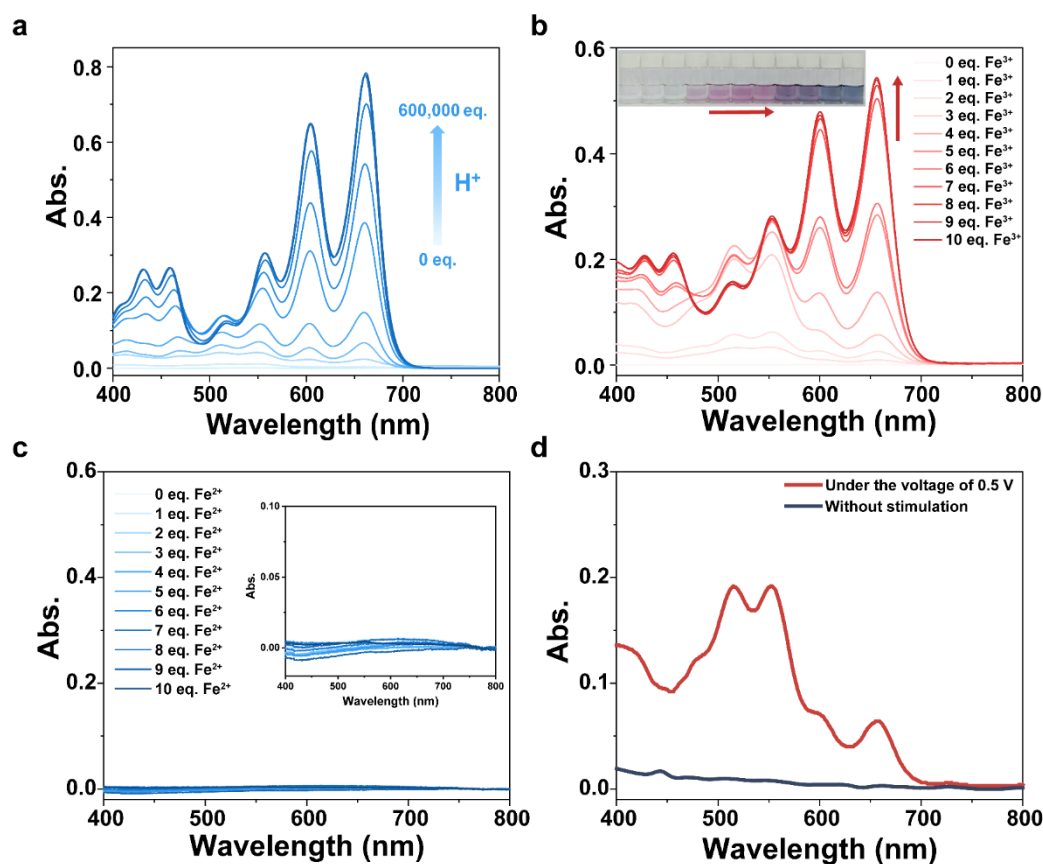


Figure 1. Feasibility of electrochromism. (a) Absorption spectra of cis-ABPX treated with various equivalents of TFA. The concentration of cis-ABPX was 1.0×10^{-5} mol/L in CHCl_3 . (b) Absorption spectra and corresponding photos (inset) of cis-ABPX treated with different equivalent FeCl_3 . The concentration of cis-ABPX was 1.0×10^{-5} mol/L in $\text{CH}_2\text{Cl}_2 + \text{CH}_3\text{CN}$ ($v:v = 1:1$). (c) Absorption spectra of cis-ABPX with various amounts of Fe^{2+} . The concentration of the solution is 1.0×10^{-5} mol/L in $\text{CH}_2\text{Cl}_2 + \text{CH}_3\text{CN}$ ($v:v = 1:1$). (d) The absorption spectra of “cis-ABPX & FeCl_2 ” without stimulation (dark blue curve) and under the voltage of 0.5 V (red curve). The concentration of cis-ABPX and FeCl_2 were 1.0×10^{-4} mol/L in $\text{CH}_2\text{Cl}_2 + \text{CH}_3\text{CN}$ ($v:v = 1:1$).

Further, the titration experiment of cis-ABPX & Fe^{3+} was performed (Figure 1b), to find Fe^{3+} could also distinguish the colored state of cis-ABPX. The color of the solution changed from colorless to magenta, then to purple and gradually to cyan with the increasing equivalent of Fe^{3+} . And surprisingly only 9 eq. of Fe^{3+} was needed to reach maximum coloration. The change progress of the absorption and fluorescence spectra were similar with the proton stimulation one (Figures 1a and S6), which indicated the lactone rings of cis-ABPX were gradually opened through coordination with Fe^{3+} . But Fe^{2+} could not achieve similar effect, the color of the mixture solution of Fe^{2+} & cis-ABPX was colorless (Figure 1c). And the results of infrared (IR) spectroscopy experiment (Figure S7) demonstrated the interaction of cis-ABPX and Fe^{3+} further. cis-ABPX had an alkane amine C-N stretching vibration peak of at 1072cm^{-1} . The C-O-C stretching vibration peak of xanthene at 1207cm^{-1} and the C-C stretching vibration peak of alkane at 1239cm^{-1} . Compared with the IR spectra of cis-ABPX or cis-ABPX & Fe^{2+} , cis-ABPX & Fe^{3+} had an asymmetric C-O-C stretching vibration peak at 1105cm^{-1} . The C-N stretching vibration peak of the tertiary amine at 1304cm^{-1} disappeared and the C=N stretching vibration peak appeared at 1649cm^{-1} . Due to the influence of O^- , the stretching vibration of carboxylic acid C=O moved towards the low wave number (1717cm^{-1}). Besides, the coordination numbers have been tested by Jobs’ plot (Figure S8). It can be found that the coordination ratio between cis-ABPX⁺ & FeCl_3 was ca. 2:3 and cis-ABPX²⁺ & FeCl_3 was ca. 1:4. In our assumption, multiple Fe^{3+} surrounded cis-ABPX⁺ and cis-ABPX²⁺, forming an dynamically ionic stabilized molecular aggregate (possibly a fragile “supramolecular cluster/cage”) [34], which not only can stabilize the configuration of cis-ABPX⁺ and cis-ABPX²⁺, but also can reduce their electrostatic repulsion. Unfortunately, due to this dynamic fragility, such supramolecular aggregates can easily undergo dynamic structural changes, it is

difficult to capture quickly by suitable testing equipment, so the inference of the dynamic structure of the “supramolecular cluster/cage” is still in the theoretical stage. We expect more researchers to join us in solving this technical problem, improve the capture speed and progress of the test instrument, and have a deeper understanding of the material structure. These results all indicated that Fe^{3+} could interact with cis-ABPX and open the lactone ring of it to change the spectra and color through the coordination interaction.

There existed difference between the interaction of Fe^{3+} & cis-ABPX and Fe^{2+} & cis-ABPX, which indicated the colors of the mixture solution of Fe^{n+} & cis-ABPX may be regulated through the electrical stimulation to develop indirect EC material. The in-situ spectro-electro-chemistry test was performed. The mixture solution of cis-ABPX and Fe^{2+} showed change in visible spectrum after treated with 0.5 V (Figure 1d), but this spectrum change was not observed in their individual solution (Figure S9). The spectra of the mixture solution demonstrated the feasibility of electrochromism here.

The states of cis-ABPX could be distinguished by the concentration of Fe^{3+} , and electrochemical experiments were conducted to determine its EC ability further. As Figure 2a shows, the oxidation potential of FeCl_2 was 0.27 V, while cis-ABPX had no redox signal at this stage. The oxidation potential ensured that FeCl_2 was oxidized before cis-ABPX, then in-situ spectro-electro-chemistry tests were conducted. The mixture solution of Fe^{2+} & cis-ABPX was nearly colorless, after applying 0.5 V, Fe^{2+} was gradually oxidized to Fe^{3+} . Then after coordination, the lactone rings of cis-ABPX were gradually opened, so the color of the mixture solution changed to magenta then to cyan. Correspondingly the absorption intensity increased at various absorption peaks, mainly located at 514 nm, 553 nm and 659 nm (Figure 2b), which was similar to cis-ABPX treated with proton (Figure 1a). However, these results were not seen in their individual solution (Figure S9). The EC mechanism based on Fe^{2+} and cis-ABPX was illustrated in Figure 2c. As the applied bias rising, Fe^{2+} began to be oxidized to Fe^{3+} to make cis-ABPX color gradually, and the absorbance of the mixture solution gradually increased. Then the color was bleached when the reduction of Fe^{3+} began. The color state of the EC system was dependent on the dynamic coordination of Fe^{n+} and cis-ABPX, and could be distinguished by the bias applied.

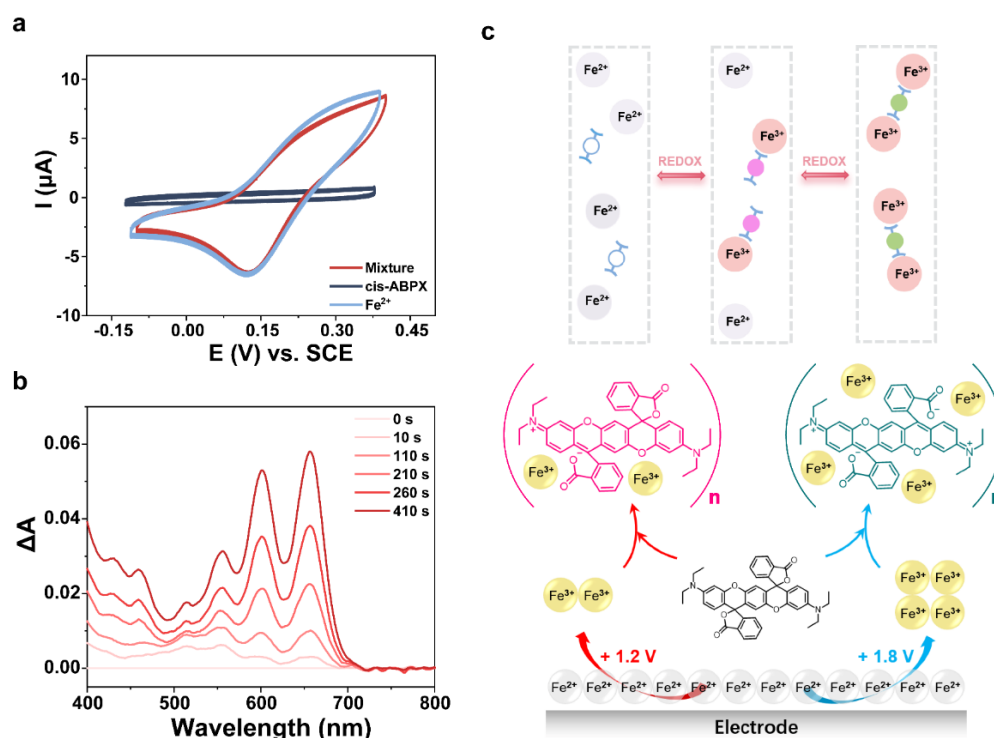


Figure 2. Investigation of the electrochromic mechanism. (a) The cyclic voltammetry curve of cis-ABPX, FeCl_2 and their mixture at 100 mV/s. The concentration of the solution was 2.0×10^{-3} mol/L in $\text{CH}_2\text{Cl}_2 + \text{CH}_3\text{CN}$ ($v:v = 1:1$). (b) The absorption spectra of “cis-ABPX + FeCl_2 ” under the voltage of 0.5 V versus Ag with different time. The concentration of cis-ABPX and FeCl_2 were 2.0×10^{-4} mol/L in $\text{CH}_2\text{Cl}_2 + \text{CH}_3\text{CN}$ ($v:v = 1:1$). (c) Illustration of the mechanism of EC processes based on cis-ABPX and Fe^{n+} .

To explore its color regulation ability further, the ECD was fabricated using the conventional “sandwich” structure (Figure 3a). The electrochromic layer was spin-coated on one indium tin oxide (ITO) glass, and ion storage layer and ion conducting layer were blade-coated on another ITO glass, then the two ITO glasses were

assembled together to fabricate the ECD (details in Experimental Part). The ECD exhibited magenta (1.2 V) and cyan (1.8 V) under different bias, then recovered to its nearly colorless state under reverse bias (Figure 3b). These results indicated the ability of Fe^{n+} to regulate the states of cis-ABPX still worked in ECD. To improve the EC performance of the device, the ratio of Fe^{2+} as redox agent and cis-ABPX as coloring agent in electrochromic layer was optimized. The molar ratio cis-ABPX: $\text{Fe}^{2+} = 4:1$ was selected for further experiment, because of the largest transmittance change (ΔT) at both 553 nm and 659 nm and the limitation of cis-ABPX solubility. It seemed that Fe^{3+} could cooperate with multiple cis-ABPX molecules in device. Then, the other components (PMMA, PC, TBAPF₆) in three layers were adjusted to optimize the EC performance. PMMA here was used as polymer matrix, PC was used as plasticizer and TBAPF₆ was used as electrolyte, their contents affected T_0 and ΔT of the device. Finally, the molar ratio PC:TBAPF₆ = 1:1 (PMMA = 50 wt%) was selected because of its largest ΔT and relatively high T_0 .

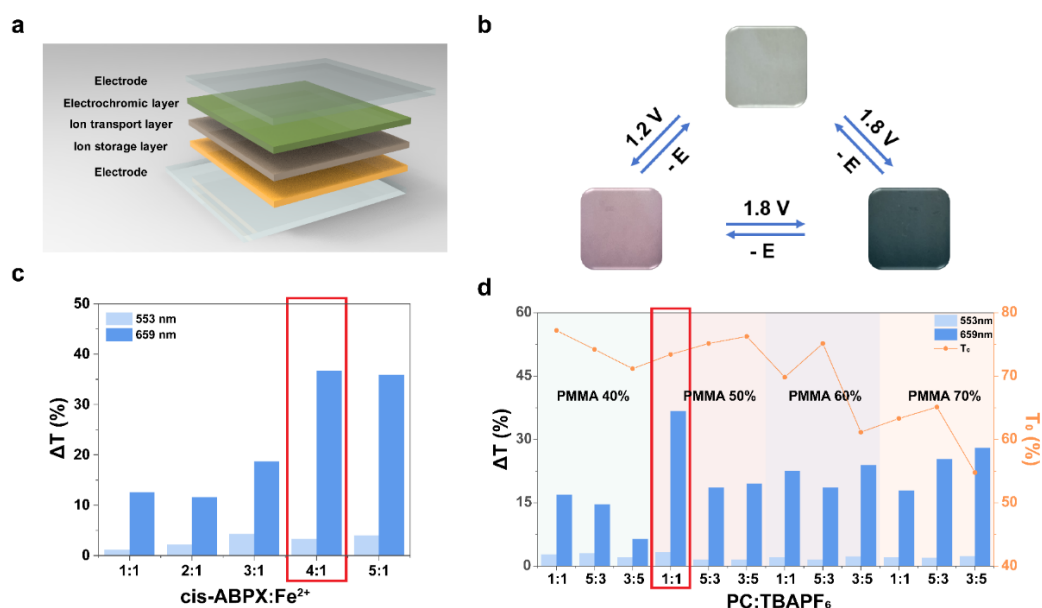


Figure 3. The optimization of the ECD. (a) The illustration of the ECD structure. (b) The photos of the device under different voltages. (c) The ΔT of the device made with different ratios of cis-ABPX/ FeCl_2 with fixed concentration of FeCl_2 (5.0×10^{-3} mol/L) under the voltage of 1.2 V, 2 s (553 nm) and 1.8 V, 2 s (659 nm). (d) The ΔT and T_0 of the device with different ratios of propylene carbonate and TBAPF₆ and different ratios of PMMA used in the electrochromic layer under the voltage of 1.2 V, 2 s (553 nm) and 1.8 V, 2 s (659 nm).

With the optimized ratio of components, the ECD was fabricated for the further tests. When different voltages were applied to the device, the transmittance of the device changed in different wavelength ranges (Figure 4a). When 1.2 V was applied, the change of transmittance mainly occurred at 500–600 nm, and the color of the corresponding device changed from colorless to magenta. Correspondingly, when 1.8 V was applied, the change of transmittance mainly occurred at 400–500 nm and 600–700 nm, and the color of the device became cyan. Colorless, magenta, cyan and their mixture could be distinguished and regulated finely by the voltage applied, as shown in Figure 4b. The CIE L * a * b * values of corresponding process in Figure 4b were listed in Table S1. The color differences were calculated to show all greater than 2, indicating the differences in Figure 4b were obvious and could be distinguished by human eyes. It took the device 7.8 s/12.3 s to color/bleach under stimulation of 1.8 V/−0.8 V respectively (Figures 4c and S10). And the ECD exhibited high CE of 185 cm²/C (Figure 4d) at 659 nm, indicating that this ECD exhibited large optical modulation under the same quantity of electric charge. The ECD could maintain the colored state for 77.1 s under open circuit with the attenuation of ΔT less than 10% (Figure S11), which has the potential to design energy-saving device. The reversibility of its coloring-bleaching cycles was measured by applying 1.7 V/−0.9 V to evaluate the service life of this ECD, ΔT showed no abnormal changes after 600 cycles (Figure S12).

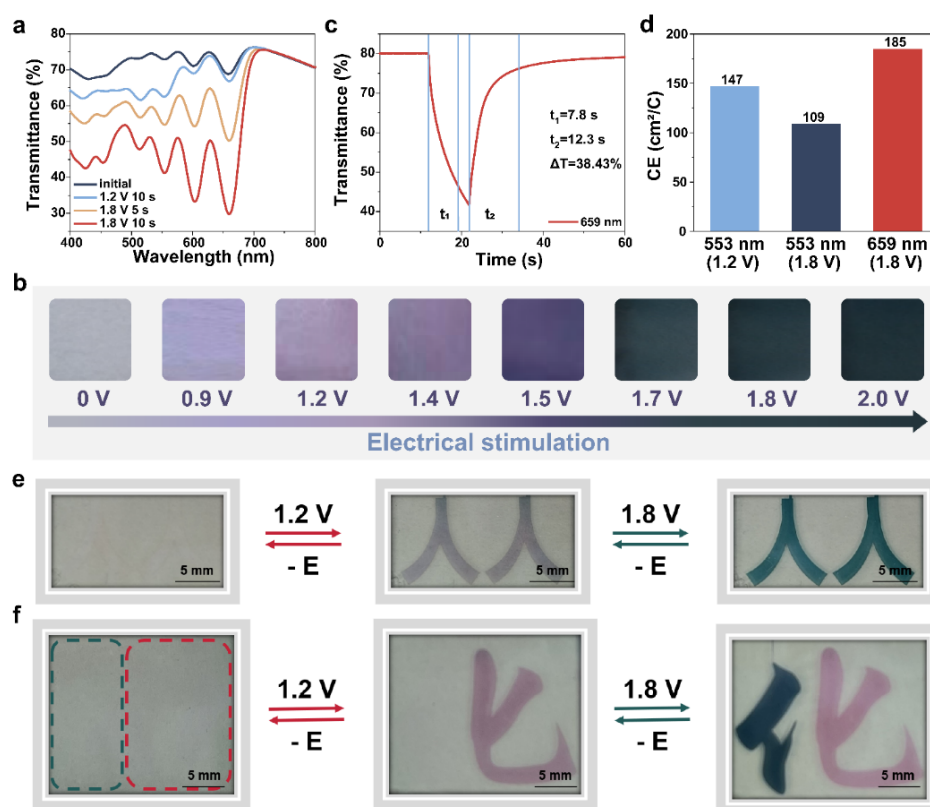


Figure 4. Investigation of the performance of the ECD. (a) The transmission spectrum of the ECD fabricated with optimal components. (b) Photos of the ECD treated with different voltage for 10 s. (c) The transmittance change at 659 nm of the ECD under the voltage of 1.8 V/−0.8 V (t_1 and t_2 corresponding to the time that takes to modulate the device transmittance from 0% to 90% of the transmittance change ratio during the coloring or fading process). (d) The CE of the ECD under different voltages and wavelengths. (e,f) The photos of the prototype ECDs under different bias (1.2 V, 30 s; 1.8 V, 15 s).

To demonstrate its intrinsic multi-color EC ability in single pixel device, prototype ECDs were fabricated (Figure 4e,f) by laser-etched ITO glass and layer-by-layer coating, the pattern was etched on the ITO glass. The color of the ECD could switch from its initial transparent colorless state to magenta state under 1.2 V, and to cyan under 1.8 V, which indicated the ability of multi-color electrochromism in single pixel (Figure 4e). Furthermore, the color of the device at different area could be switched independently. As shown in Figure 4f, after 1.2 V/1.8 V were applied to the magenta/cyan box area, the pattern showed respectively to form the Chinese character.

4. Conclusion

In conclusion, transparent colorless, magenta, cyan and various mixed color states were produced in single pixel ECD with condensed supramolecular cluster of multiple metal ions and cis-ABPX molecules and could be switched finely under different bias. This color change was based on the dynamic cooperation of multi-valent metal ion and multi-color-state molecular switch, realized intrinsic multi-color electrochromism in single cell. The EC mechanism was demonstrated by titration tests and in-situ spectro-electro-chemistry tests. The components of device were optimized and the prototype device was fabricated to demonstrate its intrinsic multi-color display ability. The low cost EC material developed here was suitable for use in low consumption reflective mode display device, and the success and grain of related exploration of intrinsically multi-color materials may probably inspire more researches to develop various other surprising applications.

Supplementary Materials: The following supporting information can be downloaded at: <https://www.sciltp.com/journals/mi/2025/1/696/s1>, Figure S1. The synthetic route for cis-ABPX; Figure S2. The ^1H NMR spectra of cis-ABPX in CDCl_3 ; Figure S3. HRMS spectrum of cis-ABPX; Figure S4. MALDI-TOF mass spectrometry of cis-ABPX; Figure S5. ^1H NMR spectra of cis-ABPX, $[\text{cis-ABPX} \& \text{H}]^+$ and $[\text{cis-ABPX} \& 2\text{H}]^{2+}$, TFA was used as proton source, and samples were dissolved in CDCl_3 ; Figure S6. The fluorescence spectra of cis-ABPX treated with excess Fe^{3+} or H^+ respectively; Figure S7. The IR spectra of cis-ABPX (black curve), cis-ABPX & Fe^{2+} (blue curve) and cis-ABPX & Fe^{3+} (red curve) in the ranges of 400 - 4000 cm^{-1} wave numbers; Figure S8. Jobs plot of cis-ABPX: FeCl_3 ; Figure S9. The absorption spectra of cis-ABPX (a) and FeCl_2 (b) without stimulation and under the voltage of 0.5 V. The concentration of cis-ABPX and FeCl_2 were 1.0×10^{-4} mol/L in $\text{CH}_2\text{Cl}_2 + \text{CH}_3\text{CN}$ (v:v = 1:1); Figure S10. The transmittance change at 553 nm of the solid-

state devices under the voltage of 1.2 V/−0.8 V (a) and 1.8 V/−0.8 V (b) (t_1 and t_2 corresponding to the time that takes to modulate the device transmittance from 0% to 90% of the transmittance change ratio during the coloring or fading process); Figure S11. The transmittance of ECD at 553 nm under stimulation of 1.2 V, power off 84.5 s, −0.8 V (a) and 1.8 V, power off 95.6 s, −1.0 V (b). (c) The transmittance of ECD at 659 nm under stimulation of 1.8 V, power off 77.1 s, −1.0 V; Figure S12. The ΔT of the ECD at 659 nm under stimulation of 1.7 V/−0.9 V for >600 test cycles, no abnormal changes; Table S1. The CIE $L^*a^*b^*$ values of the device treated with different voltages.

Author Contributions: M.L., S.W., Y.-M.Z. and S.X.-A.Z. conceived and designed this project. M.L. and S.W. wrote the original draft, S.W., Y.-M.Z. and S.X.-A.Z. revised the original draft. M.L. performed the experiments. M.L., S.W., Y.-M.Z. and S.X.-A.Z. conducted the data analysis. R.S. provided suggestions for data analysis. Y.X. provided advice for methodological. All authors have read and agreed to the published version of the manuscript.

Funding: This work was supported by China Postdoctoral Science Foundation (Grant number 2023M731273), National Natural Science Foundation of China (Grant Nos. 22475079) and the Fundamental Research Funds for the Central Universities.

Data Availability Statement: The data that support the findings of this study are available from the corresponding author upon reasonable request.

Acknowledgments: The authors thank Minjie Li, Lan Sheng and for their advices on this research. The authors thank Weiran Zhang for her kind assistance on the manuscript.

Conflicts of Interest: The authors declare that there is no conflict of interest regarding the publication of this article.

References

1. Beaujuge, P.M.; Ellinger, S.; Reynolds, J.R. The Donor–Acceptor Approach Allows a Black-to-Transmissive Switching Polymeric Electrochrome. *Nat. Mater.* **2008**, *7*, 795.
2. Rosseinsky, D.R.; Mortimer, R.J. Electrochromic Systems and the Prospects for Devices. *Adv. Mater.* **2001**, *13*, 783.
3. Grätzel, M. Ultrafast Colour Displays. *Nature* **2001**, *409*, 575.
4. Yu, H.; Qi, M.; Wang, J.; Yin, Y.; He, Y.; Meng, H.; Huang, W. A Feasible Strategy for the Fabrication of Camouflage Electrochromic Fabric and Unconventional Devices. *Electrochem. Commun.* **2019**, *102*, 31.
5. Yu, H.; Shao, S.; Yan, L.; Meng, H.; He, Y.; Yao, C.; Xu, P.; Zhang, X.; Hu, W.; Huang, W. Side-Chain Engineering of Green Color Electrochromic Polymer Materials: Toward Adaptive Camouflage Application. *J. Mater. Chem. C* **2016**, *4*, 2269.
6. Fu, H.; Yan, S.; Yang, T.; Yin, M.; Zhang, L.; Shao, X.; Dong, Y.; Li, W.; Zhang, C. New Dual Conjugated Polymer Electrochromic Device with Remarkable Yellow-to-Green Switch for Adaptive Camouflage. *Chem. Eng. J.* **2022**, *438*, 135455.
7. Sarmah, S.; Kashyap, S.S.; Bera, M.K. Dual Redox-Responsive Os/Ru-Based Alternated Heterobimetallic Supramolecular Polymer as a Multicolor Electrochromic Material for Camouflage Devices. *ACS Appl. Electron. Mater.* **2023**, *5*, 1738.
8. Laschuk, N.O.; Ebralidze, I.I.; Easton, E.B.; Zenkina, V.O. Post-Synthetic Color Tuning of the Ultra-Effective and Highly Stable Surface-Confined Electrochromic Monolayer: Shades of Green for Camouflage Materials. *ACS Appl. Mater. Interfaces* **2021**, *13*, 39573.
9. Zhao, G.; Wang, W.; Wang, X.; Xia, X.; Gu, C.; Tu, J. A Multicolor Electrochromic Film Based on a SnO₂/V₂O₅ Core/Shell Structure for Adaptive Camouflage. *J. Mater. Chem. C* **2019**, *7*, 5702.
10. Gu, C.; Yan, Y.; He, J.; Pu, D.; Chen, L.; Zhang, Y.-M.; Zhang, S.X.-A. Transparent and Energy-Efficient Electrochromic AR Display with Minimum Crosstalk Using the Pixel Confinement Effect. *Device* **2023**, *1*, 100126.
11. Kim, G.W.; Kim, Y.C.; Ko, I.J.; Park, J.H.; Bae, H.W.; Lampande, R.; Kwon, J.H. High-Performance Electrochromic Optical Shutter Based on Fluoran Dye for Visibility Enhancement of Augmented Reality Display. *Adv. Opt. Mater.* **2018**, *6*, 1701382.
12. Zhang, W.; Li, H.; Yu, W.W.; Elezzabi, A.Y. Transparent Inorganic Multicolour Displays Enabled by Zinc-Based Electrochromic Devices. *Light Sci. Appl.* **2020**, *9*, 121.
13. Wang, B.; Zhao, F.; Zhang, W.; Li, C.; Hu, K.; Carnio, B.N.; Liu, L.; Yu, W.W.; Elezzabi, A.Y.; Li, H. Inhibiting Vanadium Dissolution of Potassium Vanadate for Stable Transparent Electrochromic Displays. *Small Sci.* **2023**, *3*, 2300046.
14. Wang, Y.; Shen, R.; Wang, S.; Chen, Q.; Gu, C.; Zhang, W.; Yang, G.; Chen, Q.; Zhang, Y.-M.; Zhang, S.X.-A. A See-through Electrochromic Display via Dynamic Metal-Ligand Interactions. *Chem* **2021**, *7*, 1308.
15. Wang, Y.; Shen, R.; Wang, S.; Zhang, Y.; Zhang, S.X. Dynamic Metal–Ligand Interaction of Synergistic Polymers for Bistable See-Through Electrochromic Devices. *Adv. Mater.* **2022**, *34*, 2104413.
16. Zhao, F.; Zhao, J.; Zhang, Y.; Wang, X.; Wang, W. Self-powered quasi-solid-state electrochromic devices for optical information encryption. *J. Mater. Chem. C* **2021**, *9*, 7958.
17. Alesanco, Y.; Viñuales, A.; Palenzuela, J.; Odriozola, I.; Cabañero, G.; Rodriguez, J.; Tena-Zaera, R. Multicolor Electrochromics: Rainbow-Like Devices. *ACS Appl. Mater. Interfaces* **2016**, *8*, 14795.
18. Zhuang, Y.; Li, J.; Zhu, M.; Li, F.; Liu, S.; Zhao, Q. Electrochromism and Electrofluorochromism Based on Viologen Derivative with 1,10-Phenanthroline Moiety for Multicolor Large-Area and Patterned Display. *Adv. Mater. Technol.* **2023**, *8*, 2301092.

19. Choi, Y.; Kim, K.-W.; In, Y.R.; Tang, X.; Kim, P.; Quy, V.H.V.; Kim, Y.M.; Lee, J.; Choi, C.; Jung, C.; et al. Multicolor, Dual-Image, Printed Electrochromic Displays Based on Tandem Configuration. *Chem. Eng. J.* **2022**, *429*, 132319.
20. Song, R.; Li, G.; Zhang, Y.; Rao, B.; Xiong, S.; He, G. Novel Electrochromic Materials Based on Chalcogenoviologens for Smart Windows, E-Price Tag and Flexible Display with Improved Reversibility and Stability. *Chem. Eng. J.* **2021**, *422*, 130057.
21. Tong, Z.; Lv, H.; Zhang, X.; Yang, H.; Tian, Y.; Li, N.; Zhao, J.; Li, Y. Novel Morphology Changes from 3D Ordered Macroporous Structure to V₂O₅ Nanofiber Grassland and Its Application in Electrochromism. *Sci. Rep.* **2015**, *5*, 16864.
22. Zhang, Y.-M.; Wang, X.; Zhang, W.; Li, W.; Fang, X.; Yang, B.; Li, M.; Zhang, S.X.-A. A Single-Molecule Multicolor Electrochromic Device Generated through Medium Engineering. *Light Sci. Appl.* **2015**, *4*, e249.
23. Kim, K.-W.; Lee, J.K.; Tang, X.; Lee, Y.; Yeo, J.; Moon, H.C.; Lee, S.W.; Kim, S.H. Novel Triphenylamine Containing Poly-Viologen for Voltage-Tunable Multi-Color Electrochromic Device. *Dyes Pigment.* **2021**, *190*, 109321.
24. Wang, J.-L.; Liu, J.-W.; Sheng, S.-Z.; He, Z.; Gao, J.; Yu, S.-H. Manipulating Nanowire Assemblies toward Multicolor Transparent Electrochromic Device. *Nano Lett.* **2021**, *21*, 9203.
25. Xue, W.; Zhang, Y.; Liu, F.; Dou, Y.; Yan, M.; Wang, W. Self-powered flexible multicolor electrochromic devices for information displays. *Research* **2023**, *6*, 0227.
26. Laschuk, N.O.; Ahmad, R.; Ebralidze, I.I.; Poisson, J.; Easton, E.B.; Zenkina, O.V. Multichromic Monolayer Terpyridine-Based Electrochromic Materials. *ACS Appl. Mater. Interfaces* **2020**, *12*, 41749.
27. Malik, N.; Lahav, M.; van der Boom, M.E. Electrochromic Metallo–Organic Nanoscale Films: A Molecular Mix and Match Approach to Thermally Robust and Multistate Solid-State Devices. *Adv. Electron. Mater.* **2020**, *6*, 2000407.
28. Tsuboi, A.; Nakamura, K.; Kobayashi, N. A Localized Surface Plasmon Resonance-Based Multicolor Electrochromic Device with Electrochemically Size-Controlled Silver Nanoparticles. *Adv. Mater.* **2013**, *25*, 3197.
29. Tsuboi, A.; Nakamura, K.; Kobayashi, N. Multicolor Electrochromism Showing Three Primary Color States (Cyan–Magenta–Yellow) Based on Size- and Shape-Controlled Silver Nanoparticles. *Chem. Mater.* **2014**, *26*, 6477.
30. Wang, Z.; Wang, X.; Cong, S.; Chen, J.; Sun, H.; Chen, Z.; Song, G.; Geng, F.; Chen, Q.; Zhao, Z. Towards Full-Colour Tunability of Inorganic Electrochromic Devices Using Ultracompact Fabry-Perot Nanocavities. *Nat. Commun.* **2020**, *11*, 302.
31. Wu, M.; Li, Y.; Yuan, W.; De Bo, G.; Cao, Y.; Chen, Y. Cooperative and Geometry-Dependent Mechanochromic Reactivity through Aromatic Fusion of Two Rhodamines in Polymers. *J. Am. Chem. Soc.* **2022**, *144*, 17120.
32. Shirasaki, Y.; Okamoto, Y.; Muranaka, A.; Kamino, S.; Sawada, D.; Hashizume, D.; Uchiyama, M. Fused-Fluoran Leuco Dyes with Large Color-Change Derived from Two-Step Equilibrium: Iso-Aminobenzopyranoxanthenes. *J. Org. Chem.* **2016**, *81*, 12046.
33. Li, A.; Chu, N.; Huang, L.; Han, L.; Geng, Y.; Xu, S.; Pan, L.; Cui, H.; Xu, W.; Ma, Z. Remarkable responsive behaviors of iso-aminobenzopyranoxanthenes: Protonation effect, photochromism and piezochromism. *Dye. Pigment.* **2019**, *162*, 831.
34. Gu, C.; Wang, X.; Jia, A.-B.; Zheng, H.; Zhang, W.; Wang, Y.; Li, M.; Zhang, Y.-M.; Zhang, S.X.-A. A strategy of stabilization via active energy-exchange for bistable electrochromic displays. *CCS Chem.* **2021**, *4*, 2757.